Geometrodynamics of spinning light

KONSTANTIN Y. BLIOKH[1,2,3]*, AVI NIV[1], VLADIMIR KLEINER[1] AND EREZ HASMAN[1]

[1]Micro and Nanooptics Laboratory, Faculty of Mechanical Engineering and Russell Berrie Nanotechnology Institute, Technion–Israel Institute of Technology, Haifa 32000, Israel

[2]Institute of Radio Astronomy, 4 Krasnoznamyonnaya St., Kharkov 61002, Ukraine

[3]Nonlinear Physics Centre, Research School of Physical Sciences and Engineering, Australian National University, Canberra ACT 0200, Australia

*e-mail: k.bliokh@gmail.com

Published online: 23 November 2008; doi:10.1038/nphoton.2008.229

The semiclassical evolution of spinning particles has recently been re-examined in condensed matter physics, high-energy physics, and optics, resulting in the prediction of the intrinsic spin Hall effect associated with the Berry phase. A fundamental origin of this effect is related to the spin–orbit interaction and topological monopoles. Here, we report a unified theory and a direct observation of two mutual phenomena: a spin-dependent deflection (the spin Hall effect) of photons and the precession of the Stokes vector along the coiled ray trajectory of classical geometrical optics. Our measurements are in perfect agreement with theoretical predictions, thereby verifying the dynamical action of the topological Berry-phase monopole in the evolution of light. These results may have promising applications in nano-optics and can be immediately extrapolated to the evolution of massless particles in a variety of physical systems.

The discovery of the geometric Berry's phases in the 1980s raised interest in universal geometrical structures, such as the topological monopoles underlying the evolution of quantum particles[1,2]. The topological monopoles appear in the points of level degeneracy in parameter space, producing the Berry curvature responsible for the parallel transport of the particle state vector. In the 1990s, it was shown that the Berry phase is not a purely geometrical phenomenon, but is also a dynamical effect. As a result, the semiclassical equations of motion have been re-examined, where the Berry curvature occurs as an external field affecting the motion of the particle[3,4].

As applied to the evolution of particles with a spin, this has led to explanation of the anomalous Hall effect[5] and the prediction of the intrinsic spin Hall effect (SHE)[6,7] in semiconductor systems. For relativistic spinning particles, the Berry phase and the SHE are two manifestations of the spin–orbit interaction[8–10], which describes the mutual influence of the spin (polarization) and trajectory of the particle. In the massless case, this is associated with a topological monopole that appears in the Dirac point, that is, at the origin of momentum space[5,6,9,10]. In particular, such a situation occurs in geometrical optics of inhomogeneous media, where the SHE (also called the optical Magnus effect) has recently been predicted and examined[10–19](not to be confused with 'optical SHE' of exciton–polaritons in a semiconductor microcavity[20]).

According to theoretical predictions, a light beam propagating along a curved trajectory experiences a polarization-dependent deflection (SHE of light) caused by the spin–orbit interaction, which is solely determined by the trajectory geometry. As a result of this, even a locally isotropic inhomogeneous medium is supposed to manifest a circular birefringence of a purely topological origin[10–19]. This SHE of light in a smooth inhomogeneous medium is described by equations of motion with a 'Lorentz force' from the momentum–space topological monopole, quite similarly to the SHE in semiconductors with an applied electric field[6] and to the geometrodynamics of spinning particles in external fields[10,17,18]. This offers a unique opportunity to test fundamental equations of high-energy and condensed matter physics in an optical laboratory setting.

Despite recent experimental efforts[21–23], direct observation of the intrinsic SHE due to the topological monopole has remained an open challenge. In high-energy physics, the observation of the SHE is far beyond current experimental capabilities[10]. In condensed matter physics, direct measurements of the particle trajectories are impossible, and the situation is further complicated by competing extrinsic effects[21]. In optics, the SHE has recently been measured with great accuracy for a sharp medium inhomogeneity and a trajectory break[23], but the Berry phase formalism is inapplicable in this non-adiabatic case. (This tiny effect, also known as the Imbert–Fedorov transverse shift[24,25], has been studied over the past 50 years but has been clarified only recently; see refs 14,15 and references therein.) Thus, the fundamental semiclassical equations of motion involving the topological monopole in the momentum space have not yet been verified. Here, we report a unified theory and the first direct observation of the intrinsic SHE of light caused by the topological monopole underlying the adiabatic evolution of massless particles.

BASIC THEORY

The geometrical optics approximation for the propagation of light in an inhomogeneous medium is a counterpart of the semiclassical formalism in quantum mechanics[26]. This short-wavelength approximation requires smallness of the parameter $\mu = \lambda/L \ll 1$, where $\lambda = \lambda/2\pi$, λ is the wavelength, and L is the characteristic scale of the medium inhomogeneity. In such an approach, the propagation of light is considered as a particle-like wavepacket motion along trajectories described by the canonical formalism on the phase space $(\mathbf{p}, \mathbf{r})$. It is convenient to define the

dimensionless wave momentum as $\mathbf{p} = \lambda_0 \mathbf{k}$, with $\mathbf{k}$ being the central wavevector and $\lambda_0 = c/\omega$ (ω is the wave frequency)[26]. The parameter λ_0, which corresponds to the wavelength in vacuum, is a counterpart of the Planck constant in the semiclassical approximation.

Unlike classical point particles, electromagnetic waves have an intrinsic property—polarization or spin—which is responsible for the intrinsic angular momentum carried by light. The spin eigenstates of photons are the right-hand (R) and left-hand (L) circular polarizations denoted by the helicity $\sigma = \pm 1$. The spin angular momentum per one photon (in units of $\hbar$) equals $\sigma \mathbf{p}/p$.

In the zero-order approximation in μ (that is, in the 'classical' $\lambda \to 0$ limit of wave equations), external and internal degrees of freedom of light are uncoupled from each other. In this manner, the propagation of the electromagnetic wave is independent of the polarization, and a polarization degeneracy takes place[26]. To describe the polarization evolution of light, one has to implicate the first-order approximation, which can be regarded as 'semi-geometrical optics' akin to the semiclassical approximation in quantum mechanics. In this approximation, by taking the λ-order corrections into account, the polarization and orbital degrees of freedom become coupled with each other, which implies a spin–orbit interaction of photons[10,11].

This spin–orbit interaction can be described by the coupling Lagrangian (see Supplementary Information)

$$\mathcal{L}_{\mathrm{SOI}} = -\lambda_0 \sigma \mathbf{A}(\mathbf{p}) \dot{\mathbf{p}} \tag{1}$$

that arises under diagonalization of Maxwell equations[10,19] (cf. refs 4,6). Hereafter, the overdot stands for the derivative with respect to the ray length l. The Lagrangian (1) is reminiscent of the Lagrangian $(e/c)\mathcal{A}(\mathbf{r})\dot{\mathbf{r}}$ of a charged particle coupled with an electromagnetic field $\mathcal{A}$, but in equation (1) $\mathbf{A}(\mathbf{p})$ is the Berry vector-potential (connection) that has a purely geometrical origin[1,2]. Note that the Berry potential arises in the momentum rather than in coordinate space. This results in the generalized Euler–Lagrange equations with $\mathcal{L} = \mathcal{L}(\mathbf{p}, \dot{\mathbf{p}}, \mathbf{r}, \dot{\mathbf{r}})$ (ref. 4) corresponding to Hamiltonian dynamics with non-commutative coordinates and non-collinear velocity and momentum[3,6,10,19,27]: $\dot{\mathbf{r}} \nparallel \mathbf{p}$; see equation (5). The same Lagrangian (1) occurs under the evolution of relativistic spinning particles[10,17], and the Berry potential $\mathbf{A}(\mathbf{p})$ generates the topological monopole at the origin of momentum space[9,10,19]:

$$\mathbf{F} = \frac{\partial}{\partial \mathbf{p}} \times \mathbf{A} = \frac{\mathbf{p}}{p^3}. \tag{2}$$

The spin–orbit interaction (1) and Berry monopole (2) are of a dual geometrodynamical nature. On the one hand, the fields $\mathbf{A}$ and $\mathbf{F}$ represent the connection and curvature underlying the parallel transport of the wave electric field[28–33]. On the other hand, the Lagrangian (1) is nothing else but the Coriolis term in a wave-accompanying non-inertial coordinate frame[19,34] (see Supplementary Information).

There are two manifestations of the spin–orbit interaction of photons[11]. The first one is the influence of the trajectory upon polarization. This is the Berry phase leading to the parallel transport of the wave electric field, as predicted 70 years ago by Rytov and Vladimirskii[28,29] and examined and measured in the 1980s by Ross, Tomita, Chiao and Wu for coiled single-mode optical fibres[30–33]. The total semiclassical phase of the wave propagating along a ray trajectory ℓ is given by

$$\Phi = \lambda_0^{-1} \int_{\ell} \mathbf{p}\, \mathrm{d}\mathbf{r} - \sigma \int_{\Gamma_\ell} \mathbf{A}\, \mathrm{d}\mathbf{p}, \tag{3}$$

where Γ_ℓ is the corresponding contour of the wave evolution in the $\mathbf{p}$-space. The second term in equation (3) is the Berry phase due to the spin–orbit Lagrangian (1), which has opposite signs for R- and L-polarized waves. For elliptically polarized light, the phase difference between the R and L components determines the rotation of the polarization ellipse along the ray in accordance with the parallel transport law[28–33] (Figs 1a and 2a).

The polarization state of a fully polarized light is described by the unit three-component Stokes vector (pseudospin) $\vec{S}$ undergoing SO(3) evolution on the Poincaré (Bloch) sphere. The evolution of polarization along the ray can be written as the following precession equation for the Stokes vector[19] (see Supplementary Information):

$$\dot{\vec{S}} = \vec{\Omega} \times \vec{S}, \quad \vec{\Omega} = (0, 0, 2\mathbf{A}\dot{\mathbf{p}}). \tag{4}$$

Thus, the third component of the Stokes vector is conserved upon evolution: $S_3 = \mathrm{const}$. (Fig. 2b). Here $S_3 \in (-1, 1)$ is the mean helicity—the expectation value of the quantum helicity $\sigma = \pm 1$—and its conservation signifies the adiabatic evolution of photons.

It should be noted that the wave polarization is measured in a coordinate frame with basic vectors $(\mathbf{t}, \mathbf{v}, \mathbf{w})$ accompanying the ray, where $\mathbf{t} = \mathbf{p}/p$ is the tangent to the trajectory (Fig. 1a). Naturally, the Stokes parameters and gauge of the potential $\mathbf{A}$ depend on the choice of the basic vectors $(\mathbf{v}, \mathbf{w})$ at each point of the

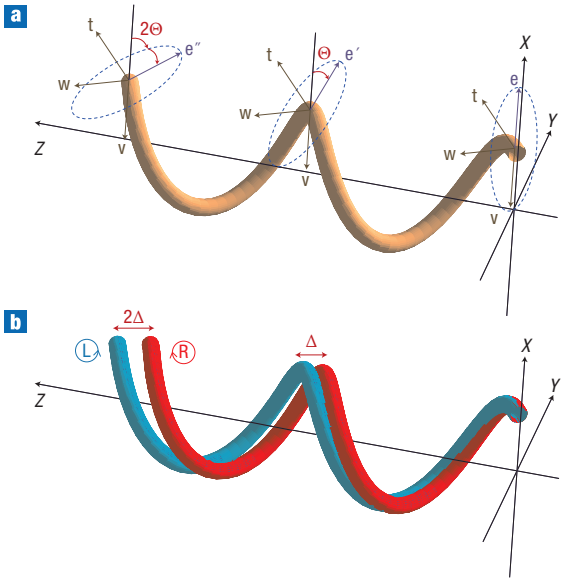

Figure 1 Spin–orbit interaction of photons—the Berry phase and spin Hall effect—on a helical light trajectory. a, The polarization ellipse evolves along a twisted ray trajectory, obeying the parallel transport law (see Fig. 2a). This effect is described by the Berry phase difference between the R- and L-polarization modes. The ray-accompanying coordinate frame is attached here to the Frenet trihedron: $(\mathbf{t}, \mathbf{v}, \mathbf{w}) = (\mathbf{t}, \mathbf{n}, \mathbf{b})$. **b**, The spin Hall effect of light. The ray trajectory is disturbed by the spin of photons, and the R- and L-polarized beams are deflected in the opposite directions.

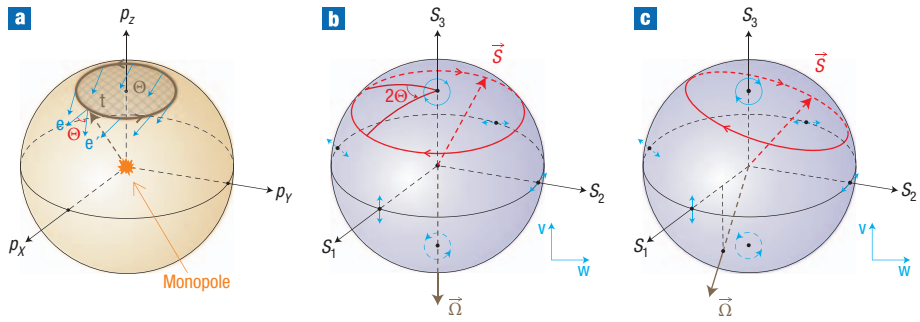

Figure 2 Representations of the evolution of the wave polarization along a helical ray trajectory. a, The parallel transport of the polarization vector $\mathbf{e}\perp\mathbf{t}$ on the unit $\mathbf{t}$ -sphere in momentum space. For a loop trajectory, the polarization is turned on the angle Θ—the solid angle enclosed by the loop. This law is associated with the topological monopole of equation (2) in the origin of momentum space. **b**, The same polarization evolution can equally be represented by the precession of the Stokes vector $\vec{S}$ on the Poincaré sphere about the S_3 axis; equation (4). **c**, In an anisotropic medium, the polarization evolution along the trajectory is described by a generalized precession of the Stokes vector on the Poincaré sphere; equation (7).

trajectory—SO(2) rotations of (**v**, **w**) produce U(1) gauge transformations of **A**. In particular, if the coordinate frame is attached to the Frenet trihedron, (**t**, **v**, **w**) = (**t**, **n**, **b**), where **n** and **b** are the normal and binormal to the ray, the ray torsion T^{-1} substitutes the quantity $-\mathbf{A}\dot{\mathbf{p}}$, so that the Berry phase equals[28–30,33] $\sigma\int_\ell T^{-1}\,dl$.

The second manifestation of the spin–orbit interaction of photons is the reciprocal influence of the polarization upon the trajectory of light. The coupling Lagrangian (1) brings about a polarization-dependent perturbation of the ray trajectories. As a result, the motion of the centre of gravity of a polarized wavepacket is described by the equations[11–14,19]

$$\dot{\mathbf{p}} = \nabla n,\ \dot{\mathbf{r}} = \frac{\mathbf{p}}{p} + \lambda_0 S_3 \dot{\mathbf{p}} \times \mathbf{F}. \qquad (5)$$

Here, $n(\mathbf{r})$ is the refractive index of the medium (which plays the role of an external scalar potential), whereas the λ-order term describes a Lorentz-type term caused by the topological monopole of equation (2). From equations (5), light beams of different polarizations propagate along slightly different trajectories; that is, an effective circular birefringence occurs in an inhomogeneous (but locally isotropic!) medium (Fig. 1b). This is the SHE of light or the optical Magnus effect, which is analogous to both the SHE of quantum particles[5–7,10] and the Magnus effect for quantum vortices[16,35]. The SHE of light was predicted by Liberman and Zel'dovich[11], and theoretically described by Bliokh and Bliokh[12,13] and Onoda, Murakami and Nagaosa[14]. As is shown in ref. 14, the topological correction in equations (5) ensures the conservation of the total angular momentum of light: $\mathbf{J} = \mathbf{r}\times\mathbf{p} + \lambda_0 S_3 \mathbf{p}/p = \text{const}$. This links the effect to a similar phenomenon of the Imbert–Fedorov transverse shift that appears under light reflection or refraction at sharp interfaces (where $\mu \propto \nabla n \to \infty$, and the adiabatic approximation is violated); see refs 14, 15 and 23 and references therein. In terms of geometric characteristics of the ray, the topological term in equations (5) takes the form $-\lambda S_3 R^{-1}\mathbf{b}$, where $\lambda = \lambda_0/p = k^{-1}$ and $R^{-1} = |\dot{\mathbf{p}}\times\mathbf{p}|/p^2$ is the curvature of the ray.

Together, equations (4) and (5) form a set of coupled equations of motion for the internal and external degrees of freedom of light. Below we aim to provide an experimental verification of the effects of the spin–orbit interaction of light, particularly of the SHE described by equations (5).

MODIFICATION FOR A CURVED REFLECTING SURFACE

The experimental realization of a spiral beam as shown in Fig. 1 in a smooth gradient-index medium is a challenging problem as it requires fabrication of the appropriate smoothly inhomogeneous sample. To circumvent this, we put forth another mechanism bending the light trajectories. Namely, we consider the light grazing a curved total internal reflection surface. The multiple total internal reflections of the light beam from a concave surface at the grazing angle result in the propagation of light along the surface. For instance, a light beam entering a glass cylinder from the end at a tangent to the surface will propagate along the cylinder surface, forming a helix similar to that in Fig. 1 (see Fig. 3). The gradient-index approximation and the first equation (5) are inapplicable in this case, because $\nabla n = \infty$ at the surface. However, the second equation (5) holds true (see Supplementary Information), and the SHE due to the topological monopole can be observed. As the light propagates along the surface, the Fermat principle implies that in the zero-order approximation the ray trajectory is a geodesic of the surface. Then, one can substitute the first equation (5) with the equation for the tangent to the geodesic. As a result we have

$$\frac{\dot{\mathbf{p}}}{p} = \frac{\mathbf{N}}{R_N}, \quad \dot{\mathbf{r}} = \frac{\mathbf{p}}{p} + \lambda_0 S_3 \frac{\dot{\mathbf{p}}\times\mathbf{p}}{p^3}. \qquad (6)$$

Here, **N** is the normal to the surface, which is directed inside the dielectric, and R_N is the radius of curvature of the surface cross-section including **t**. It is easy to see that the normal and the curvature of the surface coincide with the normal and curvature of the ray: $\mathbf{N} = \mathbf{n}$, $R_N = R$. Equations (6) represent ray equations for the geometrical-optics light propagation along a concave reflecting surface. Here the short-wavelength approximation is assured by the smallness of the parameter $\mu' = \lambda/L', L' = \min(R,T)$, similar to the case of a bent optical fibre[30–33].

The evolution of the polarization, equation (4), along a totally reflecting surface requires modification as well. The point is that the wave helicity S_3 is not conserved under the total internal reflection. Indeed, there is a phase difference that occurs between the p and s linearly polarized modes reflected from the surface[36]. By considering the grazing-angle limit of this phase difference, one can show that the wave undergoes an effective linear birefringence as in an anisotropic medium characterized by the

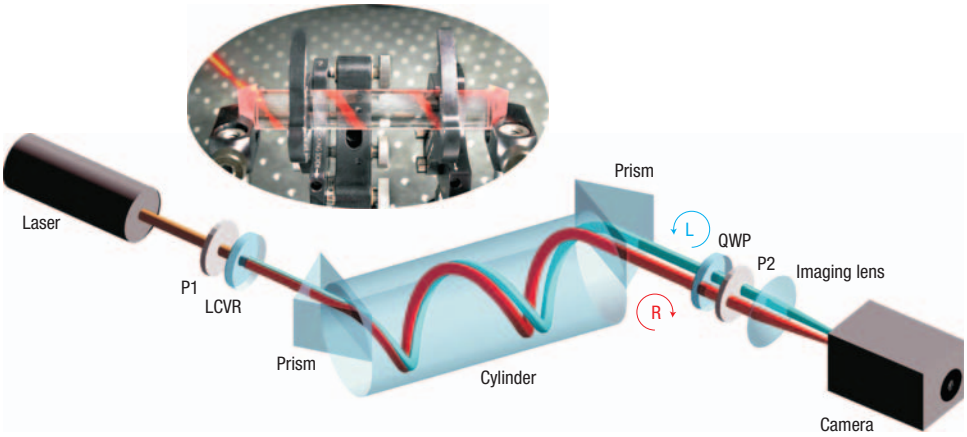

Figure 3 Experimental setup. A laser light beam enters the glass cylinder at a grazing angle through the input prism, coils along the cylinder surface, and leaves it by means of the output prism. The liquid-crystal variable retarder (LCVR) is used for generating and switching between the circularly polarized modes, whereas the quarter-wave plate (QWP) and polarizer P2 are intended for measurement of the Stokes parameters. The inset shows a real picture of the spiral light beam inside the cylinder.

phase difference $\sqrt{(1-n^{-2})}/R$ per unit ray length (see Supplementary Information). The anisotropy axes are naturally attached to the Frenet trihedron (the p and s modes are polarized along $\mathbf{n}=\mathbf{N}$ and $\mathbf{b}$, respectively), and it is convenient to write the equation for the evolution of polarization in the Frenet frame where $\mathbf{A}\dot{\mathbf{p}} \rightarrow -T^{-1}$. By introducing the phase difference between the s and p modes, we arrive at a modified precession equation for the Stokes vector[19]:

$$\dot{\vec{S}} = \vec{\Omega} \times \vec{S}, \quad \vec{\Omega} = (\sqrt{1-n^{-2}}R^{-1}, 0, -2T^{-1}). \tag{7}$$

Thus, the linear birefringence due to the total internal reflection competes with the circular birefringence due to the Berry phase, resulting in a precession of the Stokes vector about the inclined vector $\vec{\Omega}$ (Fig. 2c). The helicity is not conserved there, $S_3 \neq$ const. (which violates conservation of the total angular momentum $\mathbf{J}$), but the polarization evolution is still smooth, so that one can regard this regime as a modified adiabatic evolution. Unlike the isotropic-medium case, equations (4) and (5), the precession of the Stokes vector influences the ray deflection in equations (6) by means of varying helicity $S_3(l)$. This causes oscillations of the light trajectory that are similar to the zitterbewegung of electrons with a spin–orbit interaction[19].

EXPERIMENT

To verify the evolution equations (6) and (7), we performed an experiment involving helical light beams propagating at a grazing angle inside a glass (BK7) cylinder. The experimental setup is shown in Fig. 3. A linearly polarized HeNe laser beam at $\lambda_0 = 633$ nm wavelength was either right- or left-hand circularly polarized by a variable liquid-crystal retarder (Meadowlark Optics). The circularly polarized beam was sent at a grazing angle into a glass cylinder, using a right-angle prism fitted with an index-matching gel. We used a cylinder with radius $R_0 = 8$ mm and length $L_0 = 96$ mm and an incident beam of 1 mm width. Once inside the cylinder, the beam underwent continued internal reflections that resulted in a helical trajectory along the glass/air interface. The number of coils was adjusted by controlling the beam's angle of propagation θ between $\mathbf{t}$ and the cylinder axis. The output Stokes parameters and the beam position were measured using a polarizer, quarter-wave plate and charge-coupled device (CCD) camera (12-bit digital-cooled, PCO Sensicam 370XL, 1,280 × 1,024 pixels) imaging the outlet face of the cylinder through a second identical right-angle prism.

To calculate the output beam parameters, note that the helical ray has a constant curvature $R^{-1} = R_0^{-1}\sin^2\theta$ and torsion $T^{-1} = R_0^{-1}\sin\theta\cos\theta$. Hence, $\vec{\Omega} = \text{const}$, and equations (6) and (7) can readily be integrated (see Supplementary Information). For R- and L-polarized incident beams, $\vec{S}_{\text{in}}^{(R,L)} = (0, 0, \pm 1)$, this yields the output polarizations $\vec{S}_{\text{out}}^{(R,L)}$ and the shifts of the trajectory $\delta\mathbf{r}_{\text{out}}^{(R,L)}$:

$$\vec{S}_{\text{out}}^{(R,L)} = \pm(\omega_1\omega_3[1-\cos(\Omega l_0)], -\omega_1\sin(\Omega l_0), (1-\omega_3^2)\cos(\Omega l_0) + \omega_3^2), \tag{8}$$

$$\delta\mathbf{r}_{\text{out}}^{(R,L)} = \mp\lambda\frac{l_0}{R_0}\sin^2\theta\left[\omega_3^2 + (1-\omega_3^2)\frac{\sin(\Omega l_0)}{\Omega l_0}\right]\mathbf{b}. \tag{9}$$

where $\vec{\omega} = \vec{\Omega}/\Omega$ and $l_0 = L_0/\cos\theta$ is the total ray length in the cylinder. The relative output shift between the initially R- and L-polarized beams is $\Delta_{\text{out}} = [\delta\mathbf{r}_{\text{out}}^{(R)} - \delta\mathbf{r}_{\text{out}}^{(L)}]\mathbf{b}$. Unlike the isotropic case, Δ_{out} is a nonlinear function of the ray length l_0 due to the influence of the Stokes vector precession. The second, oscillatory term in square brackets in equation (9) describes the zitterbewegung of the light trajectory[19].

Figure 4 shows the output Stokes parameters $\vec{S}_{\text{out}}^{(R)}$ and the relative shift Δ_{out} as theoretically predicted by equations (8) and (9) and experimentally measured at different angles of propagation. The angle of propagation is expressed by the number of turns of the helix m, as $\tan\theta = 2\pi R_0 m/L_0$. An experimental error of the Stokes parameters of 0.07 was caused by the angular tolerance of the polarization elements. The number of coils m was determined to a typical accuracy of 0.2 turn. The Stokes parameters were measured using the four-measurements technique[37], and the position of the output beam was determined as a centre of mass (centroid) of the intensity distribution at the output face of the cylinder. The effects of the

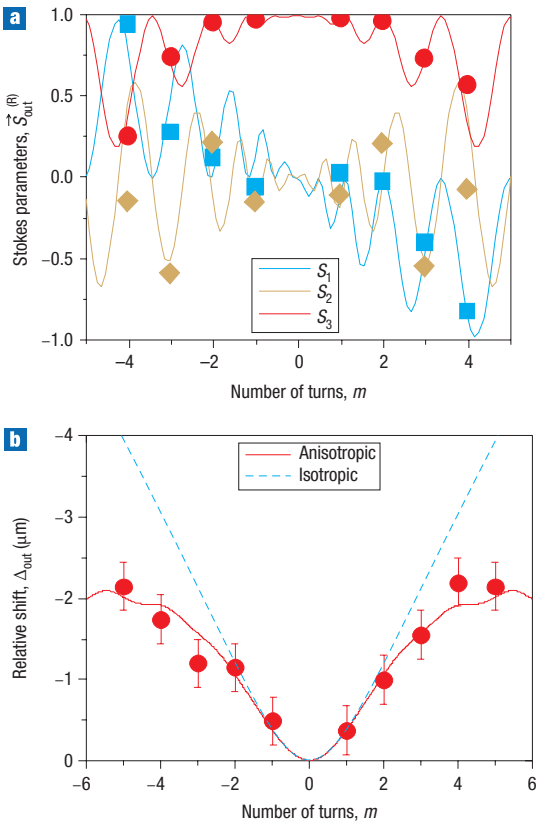

Figure 4 Experimental measurements of Stokes vector precession and the spin Hall effect of light. Calculated (curves) and measured (symbols) characteristics of the light beam, in relation to the number of turns, m, of the helical trajectory ($m < 0$ corresponds to left-handed helixes). **a**, The Stokes parameters $\vec{S}_{out}$ at the output for the R-polarized incident beam (cf. Figs 1a and 2c). The errors correspond approximately to the size of the symbols. **b**, The relative shift Δ_{out} between the output beam positions of the R and L incident beams (cf. Fig. 1b). The dashed curve indicates the shift calculated in the isotropic approximation, $S_3 = \text{const}$. The zitterbewegung variations of the beam position are noticeable at the theoretical curve for higher $|m|$. The error bars represent the typical standard deviation of the position measurements.

laser beam drift about 2 μm (typical rate 0.1 Hz) at the outlet face of the cylinder were minimized by taking alternating readings between the two circular polarizations at a rate of 1 Hz and averaging over 40 measurements. Such a technique reduced the errors due to statistical noise and, as a result, the relative shift Δ_{out} was determined to a typical accuracy of 0.3 μm. Systematic errors caused by a non-normal beam incidence on the prism (the angle of incidence being up to 25°) are negligible against a background of the above statistical errors.

The experimental measurements fully confirm all the theoretical predictions. The Stokes vector precession, the spin Hall effect, and the effect of the anisotropy on the shift Δ_{out} are clearly seen in Fig. 4.

CONCLUSION

We have presented a unified theory and a direct observation of the spin Hall effect of light and of the Stokes-vector precession in an effectively inhomogeneous and anisotropic medium. Both the effects arise from the spin–orbit interaction of photons and the topological monopole in Maxwell equations. Although the Berry phase and the parallel transport of polarization along the ray could be regarded as a purely geometrical phenomenon (it disappears in the proper parallel-transported coordinate frame), the SHE of light allows a natural dynamical explanation and occurs independently of the coordinate frame. Together, these two effects reveal in-depth geometrodynamical interrelations underlying the evolution of spinning particles in external fields. Because of the close similarity and common topological roots of the SHE in optics, condensed matter and high-energy physics, one can regard our results as indirect evidence of the intrinsic SHE in a diversity of physical systems.

In addition to the fundamental interest in it, the SHE has a potential application as a novel type of particle transport. Our experiment, as well as the recent experiment in ref. 23, indicates that optical systems have an advantage over condensed-matter systems because of the relative purity and simplicity of the optical components. Also, the magnitude of the SHE of light can be substantially enhanced by involving higher-order angular-momentum states of light—optical vortex beams[16]. (Note, however, that vortex-induced transport does not occur for the total reflection used in our experiment[38].) In general, introducing spin–orbit coupling of electromagnetic waves into contemporary photonics and nano-optics may result in the development of a promising new area of research—spinoptics.

Received 29 August 2008; accepted 23 October 2008;
published 23 November 2008.

References

1. Berry, M. V. Quantal phase-factors accompanying adiabatic changes. *Proc. R. Soc. A* **392,** 45–57 (1984).
2. Shapere, A. & Wilczek, F. (eds) *Geometric Phases in Physics* (World Scientific, 1989).
3. Littlejohn, R. G. & Flynn, W. G. Geometric phases in the asymptotic theory of coupled wave-equations. *Phys. Rev. A* **44,** 5239–5256 (1991).
4. Sundaram, G. & Niu, Q. Wave-packet dynamics in slowly perturbed crystals: Gradient corrections and Berry-phase effects. *Phys. Rev. B* **59,** 14915–14925 (1999).
5. Fang, Z. *et al.* The anomalous Hall effect and magnetic monopoles in momentum space. *Science* **302,** 92–95 (2003).
6. Murakami, S., Nagaosa, N. & Zhang, S. C. Dissipationless quantum spin current at room temperature. *Science* **301,** 1348–1351 (2003).
7. Sinova, J. *et al.* Universal intrinsic spin Hall effect. *Phys. Rev. Lett.* **92,** 126603 (2004).
8. Mathur, H. Thomas precession, spin–orbit interaction and Berry's phase. *Phys. Rev. Lett.* **67,** 3325–3327 (1991).
9. Bialynicki-Birula, I. & Bialynicki-Birula, Z. Berry's phase in the relativistic theory of spinning particles. *Phys. Rev. D* **35,** 2383–2387 (1987).
10. Bérard, A. & Mohrbach, H. Spin Hall effect and Berry phase of spinning particles. *Phys. Lett. A* **352,** 190–195 (2006).
11. Liberman, V. S. & Zel'dovich, B. Y. Spin–orbit interaction of a photon in an inhomogeneous medium. *Phys. Rev. A* **46,** 5199–5207 (1992).
12. Bliokh, K. Y. & Bliokh, Y. P. Modified geometrical optics of a smoothly inhomogeneous isotropic medium: The anisotropy, Berry phase and the optical Magnus effect. *Phys. Rev. E* **70,** 026605 (2004).
13. Bliokh, K. Y. & Bliokh, Y. P. Topological spin transport of photons: the optical Magnus effect and Berry phase. *Phys. Lett. A* **333,** 181–186 (2004).
14. Onoda, M., Murakami, S. & Nagaosa, N. Hall effect of light. *Phys. Rev. Lett.* **93,** 083901 (2004).
15. Bliokh, K. Y. & Bliokh, Y. P. Conservation of angular momentum, transverse shift and spin Hall effect in reflection and refraction of an electromagnetic wave packet. *Phys. Rev. Lett.* **96,** 073903 (2006).
16. Bliokh, K. Y. Geometrical optics of beams with vortices: Berry phase and orbital angular momentum Hall effect. *Phys. Rev. Lett.* **97,** 043901 (2006).
17. Duval, C., Horváth, Z. & Horváthy, P. A. Fermat principle for spinning light. *Phys. Rev. D* **74,** 021701(R) (2006).
18. Gosselin, P., Bérard, A. & Mohrbach, H. Spin Hall effect of photons in a static gravitational field. *Phys. Rev. D* **75,** 084035 (2007).
19. Bliokh, K. Y., Frolov, D. Y. & Kravtsov, Y. A. Non-Abelian evolution of electromagnetic waves in a weakly anisotropic inhomogeneous medium. *Phys. Rev. A* **75,** 053821 (2007).
20. Leyder, C. *et al.* Observation of the optical spin Hall effect. *Nature Phys.* **3,** 628–631 (2007).
21. Kato, Y. K., Myers, R. C., Gossard, A. C. & Awschalom, D. D. Observation of the spin Hall effect in semiconductors. *Science* **306,** 1910–1913 (2004).
22. Wunderlich, J., Kaestner, B., Sinova, J. & Jungwirth, T. Experimental observation of the spin-Hall effect in a two-dimensional spin–orbit coupled semiconductor system. *Phys. Rev. Lett.* **94,** 047204 (2005).
23. Hosten, O. & Kwiat, P. Observation of the spin Hall effect of light via weak measurements. *Science* **319,** 787–790 (2008).
24. Fedorov, F. I. K teorii polnogo otrazheniya. *Dokl. Akad. Nauk SSSR* **105,** 465–468 (1955).
25. Imbert, C. Calculation and experimental proof of transverse shift induced by total internal reflection of a circularly polarized-light beam. *Phys. Rev. D* **5,** 787–796 (1972).
26. Kravtsov, Y. A. & Orlov, Y. I. *Geometrical Optics of Inhomogeneous Medium* (Springer-Verlag, 1990).
27. Kuratsuji, H. & Iida, S. Deformation of symplectic structure and anomalous commutators in field theories. *Phys. Rev. D* **37,** 441–447 (1988).
28. Rytov, S.M. Dokl. Akad. Nauk. SSSR **18,** 263–265 (1938). Reprinted in Markovski, B. & Vinitsky, S. I. (eds) *Topological Phases in Quantum Theory* (World Scientific, 1989).
29. Vladimirskii, V. V. Dokl. Akad. Nauk. SSSR **31,** 222–224 (1941). Reprinted in Markovski, B. & Vinitsky, S. I. (eds) *Topological Phases in Quantum Theory* (World Scientific, 1989).

30. Ross, J. N. The rotation of the polarization in low birefringence monomode optical fibres due to geometric effects. *Opt. Quant. Electron.* **16,** 455–461 (1984).
31. Chiao, R. Y. & Wu, Y. S. Manifestations of Berry topological phase for the photon. *Phys. Rev. Lett.* **57,** 933–936 (1986).
32. Tomita, A. & Chiao, R. Y. Observation of Berry topological phase by use of an optical fiber. *Phys. Rev. Lett.* **57,** 937–940 (1986).
33. Berry, M. V. Interpreting the anholonomy of coiled light. *Nature* **326,** 277–278 (1987).
34. Lipson, S. G. Berry's phase in optical interferometry— a simple derivation. *Opt. Lett.* **15,** 154–155 (1990).
35. Thouless, D. J., Ao, P. & Niu, Q. Transverse force on a quantized vortex in a superfluid. *Phys. Rev. Lett.* **76,** 3758–3761 (1996).
36. Born, M. & Wolf, E. *Principles of Optics* Ed. 6 (Pergamon, 1980).
37. Collet, E. *Polarized Light* (Marcel Dekker, 1993).
38. Fedoseev, V. G. Spin-independent transverse shift of the centre of gravity of a reflected and of a refracted light beam. *Opt. Commun.* **193,** 9–18 (2001).

Supplementary Information accompanies this paper at www.nature.com/naturephotonics.

Acknowledgements

We are indebted to P.A. Horváthy, C. Duval and Y.A. Kravtsov for fruitful correspondence. The work by K.B. is supported by the Linkage International Grant of the Australian Research Council.

Author information

Reprints and permission information is available online at http://npg.nature.com/reprintsandpermissions/.
Correspondence and requests for materials should be addressed to K.Y.B.